Monthly Notices
of the
ROYAL ASTRONOMICAL SOCIETY

MNRAS **474,** 1288–1295 (2018)
Advance Access publication 2017 October 26

doi:10.1093/mnras/stx2790

Sub-structure formation in starless cores

C. Toci,[1,2]★ D. Galli,[1,2]★ A. Verdini,[1,2] L. Del Zanna[1,2,3] and S. Landi[1,2]

[1] *Università degli Studi di Firenze, Via G. Sansone 1, I-50019 Sesto Fiorentino, Italy*
[2] *INAF – Osservatorio Astrofisico di Arcetri, Largo E. Fermi 5, I-50125 Firenze, Italy*
[3] *INFN – Sezione di Firenze, Via G. Sansone 1, I-50019 Sesto Fiorentino, Italy*

Accepted 2017 October 24. Received 2017 October 24; in original form 2017 August 8

ABSTRACT

Motivated by recent observational searches of sub-structure in starless molecular cloud cores, we investigate the evolution of density perturbations on scales smaller than the Jeans length embedded in contracting isothermal clouds, adopting the same formalism developed for the expanding Universe and the solar wind. We find that initially small amplitude, Jeans-stable perturbations (propagating as sound waves in the absence of a magnetic field) are amplified adiabatically during the contraction, approximately conserving the wave action density, until they either become non-linear and steepen into shocks at a time $t_{\rm nl}$, or become gravitationally unstable when the Jeans length decreases below the scale of the perturbations at a time $t_{\rm gr}$. We evaluate analytically the time $t_{\rm nl}$ at which the perturbations enter the non-linear stage using a Burgers' equation approach, and we verify numerically that this time marks the beginning of the phase of rapid dissipation of the kinetic energy of the perturbations. We then show that for typical values of the rms Mach number in molecular cloud cores, $t_{\rm nl}$ is smaller than $t_{\rm gr}$, and therefore density perturbations likely dissipate before becoming gravitational unstable. Solenoidal modes grow at a faster rate than compressible modes, and may eventually promote fragmentation through the formation of vortical structures.

Key words: hydrodynamics – ISM: clouds – ISM: kinematics and dynamics.

1 INTRODUCTION

The growth of small-scale density perturbations during the collapse of an interstellar cloud has been the subject of many studies aimed at understanding the formation of stellar clusters and multiple stellar system by the process of fragmentation, namely the break-up of a large cloud into clumps, cores and stellar clusters. While early studies (Hunter 1962, 1964; Mestel 1965a,b) focused on the growth of initially Jeans-unstable perturbations, Tohline (1980) introduced the concept of 'delayed fragmentation', as the onset of gravitational instability can occur only after the mean density of the cloud (assumed to be in free-fall collapse) has grown significantly, and the instantaneous value of the Jeans length has become smaller than the scale of the perturbed region. Tohline (1980) argued that in this case the time needed for a significant amplification of the perturbations would be larger than the time the parent cloud has left in its evolution, and pointed out the role of the converging motion of the gas, in alternative to self-gravity, as a means to amplify small-scale density perturbations that are initially Jeans-stable. The fate of these initially Jeans-stable perturbations was investigated numerically in collapse simulations by Rozyczka (1983), who found them subject to efficient damping well before reaching the threshold for gravitational instability, and therefore unable to form well-defined fragments. Furthermore, in his simulations Rozyczka (1983) observed the formation of local concentrations of angular momentum (possibly as the result of tidal interactions) even in the collapse of initially non-rotating clouds. Whether these local enhancements of vorticity would turn themselves into turbulent eddies, as originally suggested by Layzer (1963), or eventually evolve to rotationally supported disc-like structures, as suggested, for example, by the simulations by Goodwin, Whitworth & Ward-Thompson (2004), has remained unclear.

Recently, an original approach to the problem of the growth of density perturbations embedded in a collapsing cloud was adopted by Toalà et al. (2015), who formulated the problem in the framework of an *inverse Hubble flow*, i.e. the gravitational collapse of a spherical pressureless cloud, exploiting the analytical tools developed in cosmology for the expanding Universe.[1] Toalà et al. (2015) found that the gravitational instability occurs faster in inverse Hubble flows than in a static cloud, and postulated that growing, unstable perturbations on scales larger than the Jeans length $\lambda_{\rm J}$ collapse when they reach the non-linear stage, i.e. at a time $t_{\rm nl}$ identified by the condition $\delta\rho/\rho \approx 1$. In inverse Hubble flows, $t_{\rm nl}$ is always smaller

★ E-mail: claudia@arcetri.astro.it (CT); galli@arcetri.astro.it (DG)

[1] In cosmology, this solution corresponds to the Lemaitre–Tolman elliptic ($k = +1$) solution of Einstein's equations for a 'dust' Universe

than the free-fall time $t_{\rm ff}$ of the cloud, and approaches the latter in the limit of initially small amplitude of the perturbations.

While Toalà et al. (2015) studied the evolution of Jeans-unstable perturbations in a cloud containing a large number of Jeans masses, in this work, we consider molecular cloud cores containing only a few Jeans masses, and focus on the evolution of Jeans-stable density perturbations, that initially oscillate as a collection of sound waves of small amplitude. This is justified by the observational result that non-thermal motions in dense cores are generally subsonic (Myers 1983). In the case of starless cores, it has been suggested that subsonic motions ('turbulence') may be forming the seeds of multiple sites of star formation (Fisher 2004, Goodwin et al. 2004, Goodwin et al. 2007), but scarce evidence has been found yet for sub-structure formation in these objects (Schnee et al. 2012, Dunham et al. 2016). For example, Schnee et al. (2012) examined four 'super-Jeans' starless cores of masses 3–8 $M_\odot$ finding upper limits on the masses of any embedded fragment down to a few thousandths of solar mass. Only recently some evidence of compact sub-structure has been found in one starless core in Ophiuchus (Kirk et al. 2017) and in the Orion Molecular Cloud 1 South (Palau et al. 2017). In any case, the processes determining the formation of multiple protostellar seeds at these scales remain unclear.

To address the problem of sub-structure formation in cloud cores, in this paper, we investigate the evolution of density and velocity perturbations embedded in a contracting medium (the 'background' or 'parent cloud') undergoing isotropic or anisotropic collapse. First, we formulate a theoretical framework to study contracting flows based on methods developed in cosmology for the expanding Universe (see e.g. Peebles 1980) and in the study of the expanding solar wind (Grappin, Velli & Mangeney 1993; Grappin & Velli 1996; Tenerani & Velli 2013; Dong, Verdini & Grappin 2014; Verdini & Grappin 2015). In this framework, we study analytically the linear and non-linear evolution of perturbations. We consider two simple cases of contracting backgrounds: a spherical cloud undergoing homologous pressureless collapse and the spherical accretion flow on a point mass.

Related problems are the evolution of oscillations in contracting cores (Broderick & Keto 2010; Keto & Caselli 2010), and the behaviour of hydrodynamical turbulence during the contraction of a cloud (Robertson & Goldreich 2012; Davidovits & Fish 2017). The latter studies, in particular, demonstrates that the root-mean-square (rms) turbulent velocity increases during contraction, as long as the eddy turnover time is shorter than the contraction time (a process termed 'adiabatic heating' of turbulence).

The paper is organized as follows: In Section 2, we formulate the equations of hydrodynamics in comoving coordinates for application to contracting interstellar clouds; in Section 3, we study the evolution of linear perturbations in the case of isotropic and anisotropic contraction; in Section 4, we apply the formalism of inverse Hubble flows to the homologous collapse of a uniform-density cloud; in Section 5, we compare our analytical results to a hydrodynamical simulation in a contracting box. Finally, in Section 6, we summarize our conclusions.

2 HYDRODYNAMICS IN COMOVING COORDINATES

To investigate the dynamics of contracting clouds, we employ an approach similar to the one commonly used in cosmological studies, where a background medium evolves with some specified laws (the Friedmann equations in that case) and the growth of primordial perturbations is followed in a local coordinate system comoving with the background flow. We generalize this approach by relaxing the assumption of an isotropic expansion/contraction. Given the non-uniformity of the interstellar medium, characterized by a filamentary structure and the presence of accretion flows, fluid motions are not expected to be isotropic. For example, a fluid element accreting on to a mass point is accelerating and stretching in the direction of the flow, while contracting in the transverse directions.[2]

Consider a small Cartesian line element $\delta\boldsymbol{x} = (\delta x, \delta y, \delta z)$ advected by the flow, evolving as

$$\delta\boldsymbol{x}(t) = \mathbb{S}(t)\cdot\delta\boldsymbol{x}_0, \tag{1}$$

where $\mathbb{S}(t) = \mathrm{diag}[a(t), b(t), c(t)]$ is the scalefactor normalized such that $\mathbb{S}(t_0) = \mathbb{I}$ and $\delta\boldsymbol{x}(t_0) = \delta\boldsymbol{x}_0$. All hydrodynamical quantities can be written as the sum of background and local components (hereafter 'perturbations'), as

$$\boldsymbol{u} = \boldsymbol{u}_{\rm b} + \boldsymbol{u}_1, \quad \rho = \rho_{\rm b} + \rho_1, \tag{2}$$

where $\boldsymbol{u}(\boldsymbol{x}, t)$ is the velocity field, $\rho(\boldsymbol{x}, t)$ is the gas density and $\boldsymbol{x} = (x, y, z)$. In the following, we assume an isothermal equation of state $p = c_{\rm s}^2\rho$, where p is the gas pressure and $c_{\rm s}$ is the (constant) sound speed. We also assume that the background density is spatially uniform. The background velocity then follows a Hubble-type law,

$$\boldsymbol{u}_{\rm b}(\boldsymbol{x}, t) = \mathbb{H}(t)\cdot\boldsymbol{x}, \tag{3}$$

where $\mathbb{H}(t) = \mathrm{diag}(\dot{a}/a, \dot{b}/b, \dot{c}/c)$, and the equation of continuity implies

$$\rho_{\rm b}(t) = \frac{\rho_0}{abc}, \tag{4}$$

where $\rho_0 = \rho_{\rm b}(t_0)$ is the initial value of the background density. Let us introduce a system of comoving coordinates

$$\boldsymbol{x}' = \mathbb{S}^{-1}(t)\cdot\boldsymbol{x}. \tag{5}$$

in which the line element advected by the background flow appears stationary. In these comoving coordinates the hydrodynamical equations become

$$\frac{\partial\rho_1}{\partial t} + \tilde{\nabla}\cdot(\rho\boldsymbol{u}_1) = -\mathrm{tr}\mathbb{H}\,\rho_1, \tag{6}$$

and

$$\frac{\partial_{+1}}{\partial t} + (\boldsymbol{u}_1\cdot\tilde{\nabla})\boldsymbol{u}_1 + \frac{c_{\rm s}^2}{\rho}\tilde{\nabla}\rho_1 + \boldsymbol{g}_1 = -\mathbb{H}\cdot\boldsymbol{u}_1, \tag{7}$$

where the spatial gradient $\tilde{\nabla}$ is

$$\tilde{\nabla} = \frac{1}{a}\frac{\partial}{\partial x'}\hat{\boldsymbol{e}}_x + \frac{1}{b}\frac{\partial}{\partial y'}\hat{\boldsymbol{e}}_y + \frac{1}{c}\frac{\partial}{\partial z'}\hat{\boldsymbol{e}}_z = \mathbb{S}^{-1}\cdot\nabla', \tag{8}$$

and the gravitational field $\boldsymbol{g}_1$ satisfies Poisson's equation

$$\tilde{\nabla}\cdot\boldsymbol{g}_1 = 4\pi G\rho_1. \tag{9}$$

3 LINEAR EVOLUTION OF PERTURBATIONS

The linearized equations are

$$\frac{\partial\delta}{\partial t} + \tilde{\nabla}\cdot\boldsymbol{u}_1 = 0, \tag{10}$$

[2] In the case of the solar wind, expanding at different rates in the radial and transverse directions, a similar formalism is called 'expanding box model' (Grappin et al. 1993; Grappin & Velli 1996).

and

$$\frac{\partial +_1}{\partial t} + c_s^2 \tilde{\nabla}\delta + \boldsymbol{g}_1 = -\mathbb{H}\cdot\boldsymbol{u}_1. \tag{11}$$

where $\delta(\boldsymbol{x}', t) = \rho_1(\boldsymbol{x}', t)/\rho_b(t)$ is the density contrast. Taking the curl ($\tilde{\nabla}\times$) of equation (11), we obtain the evolution of the vorticity $\boldsymbol{\omega}_1 = \tilde{\nabla}\times\boldsymbol{u}_1$,

$$\frac{\partial \boldsymbol{\omega}_1}{\partial t} = -\mathrm{tr}\mathbb{H}\,\boldsymbol{\omega}_1 + \mathbb{H}\cdot\boldsymbol{\omega}_1, \tag{12}$$

showing that any initial vorticity is enhanced by the contraction of the cloud ($\mathbb{H} < 0$). If the contraction is isotropic, equation (12) reduces to

$$\frac{\partial \boldsymbol{\omega}_1}{\partial t} = -2\frac{\dot{a}}{a}\boldsymbol{\omega}_1, \tag{13}$$

showing the vorticity increases as $a(t)^{-2}$, the reverse of the so-called 'natural decay' of vorticity in the expanding Universe. A more general form of equation (13) for the mean vorticity $\langle\boldsymbol{\omega}^2\rangle^{1/2}$ has been obtained by Olson & Sachs (1973), who included a non-linear term representing the break-up of larger eddies into smaller ones in incompressible turbulence (a process that tends to increase the mean vorticity). While in the expanding Universe the latter process competes with the 'natural decay' due to the overall expansion, in a contracting cloud it always leads to an unbounded increase of the mean vorticity that blows up in a finite time, if the fluid has zero viscosity (Olson & Sachs 1973). These ideas have been expanded by Robertson & Goldreich (2012).

Taking the divergence ($\tilde{\nabla}\cdot$) on both sides of equation (11) and using equation (10), we obtain the evolutionary equation for compressible modes (that couple to gravity)

$$\frac{\partial^2\delta}{\partial t^2} - c_s^2\tilde{\nabla}^2\delta - 4\pi G\rho_b\delta = 2\tilde{\nabla}\cdot(\mathbb{H}\cdot\boldsymbol{u}_1). \tag{14}$$

Consider a single Fourier mode with amplitude

$$\delta(\boldsymbol{x}', t) = F(t)e^{i\boldsymbol{k}'\cdot\boldsymbol{x}'}, \tag{15}$$

where $\boldsymbol{k}'$ is the (constant) comoving wavevector, related to the proper (time-dependent) wavevector $\boldsymbol{k}(t)$ by

$$\boldsymbol{k}(t) = \mathbb{S}^{-1}(t)\boldsymbol{k}'. \tag{16}$$

Inserting this expression in equation (14), we obtain

$$\frac{\mathrm{d}^2F}{\mathrm{d}t^2} + 2H\frac{\mathrm{d}F}{\mathrm{d}t} + c_s^2(k^2 - k_J^2)F = 0, \tag{17}$$

where $k = |\boldsymbol{k}|$,

$$H = \frac{1}{k^2}\left(\frac{\dot{a}}{a}k_x^2 + \frac{\dot{b}}{b}k_y^2 + \frac{\dot{c}}{c}k_z^2\right) = -\frac{1}{k}\frac{\mathrm{d}k}{\mathrm{d}t} \tag{18}$$

is the contraction rate, and

$$k_J(t) = \frac{\sqrt{4\pi G\rho_b(t)}}{c_s} \equiv \frac{k_{J,0}}{\sqrt{abc}} \tag{19}$$

is the Jeans wavenumber. The effect of the contraction is to decrease the wavelength $\lambda(t) = 2\pi/k(t)$ and increase the amplitude (second term on the LHS, with $H < 0$) of perturbations. If the compression rate in one direction is much larger than in the other two, perturbations grow faster along that direction and become asymptotically two dimensional. The wavevector of the perturbations, fixed in comoving coordinates, in physical space becomes progressively aligned with the direction of stronger compression.

Defining the variable ξ as

$$\frac{\mathrm{d}\xi}{\mathrm{d}t} = c_s\frac{k^2(t)}{k_{J,0}^2} \tag{20}$$

equation (17) can be written in compact form as

$$\frac{\mathrm{d}^2F}{\mathrm{d}\xi^2} + \left(\frac{k_{J,0}}{k}\right)^4(k^2 - k_J^2)F = 0, \tag{21}$$

which generalises the 'basic equation of fragmentation theory' by Lynden-Bell (1973).

3.1 Wkb approximation

If $k > k_J$ perturbations oscillate. If the oscillation period is much smaller than the contraction time, the amplitude of perturbations can be estimated by a WKB analysis (see e.g. Falle 1972). Assuming

$$F(\xi) = f(\xi)e^{-i\phi(\xi)} \tag{22}$$

with $\phi(\xi)$ oscillating on a time-scale much smaller than variation of $f(\xi)$, the dominant terms in equation (21) can be eliminated by choosing

$$\frac{\mathrm{d}\phi}{\mathrm{d}\xi} = \left(\frac{k_{J,0}}{k}\right)^2(k^2 - k_J^2)^{1/2}, \tag{23}$$

whereas the next largest terms give the condition

$$f\frac{\mathrm{d}^2\phi}{\mathrm{d}\xi^2} + 2\frac{\mathrm{d}f}{\mathrm{d}\xi}\frac{\mathrm{d}\phi}{\mathrm{d}\xi} = 0, \tag{24}$$

which implies $f^2\,d\phi/d\xi = $ constant. From equation (23), one then obtains

$$f \propto \frac{k}{(k^2 - k_J^2)^{1/4}}. \tag{25}$$

For $k \gg k_J$, equation (22) represents oscillations with instantaneous frequency

$$\omega(t) = \frac{\mathrm{d}\varphi}{\mathrm{d}t} \approx c_s k(t) \tag{26}$$

and amplitude increasing as $k(t)^{1/2}$. If the contraction is isotropic with scalefactor $a(t)$ the period of the oscillations ($k^{-1} \propto a$) becomes progressively smaller than the time-scale of the variation of the amplitude ($k^{1/2} \propto a^{-1/2}$), thus making the WKB approximation valid at any time, if it is satisfied initially, whereas in cosmology the WKB approximation is satisfied only at early times (see e.g. Peebles 1980). Similarly, a WKB analysis of equation (10) shows that $|\boldsymbol{u}_1| = c_s\delta \propto a^{-1/2}$. In this approximation, compressible modes conserve the action density

$$\frac{\mathcal{E}(t)}{\omega(t)} = \text{constant}, \tag{27}$$

where

$$\mathcal{E}(t) = \frac{1}{2}c_s^2\delta^2 + \frac{1}{2}|\boldsymbol{u}_1|^2 = c_s^2\delta^2 \tag{28}$$

is the energy density of the perturbations (Bretherton & Garrett 1968; Dewar 1970).

3.2 Special case: free-fall on a point mass

As an application, we evaluate the amplification of small-scale perturbations ($k \gg k_J$) during spherical free-fall on a star of mass $M_\star$. In this case, the fluid element experiences a compression in the transverse directions, say x, y, and a stretching in the radial direction, say z,

$$a(t) = b(t) = \cos^2\mu(t) \qquad c(t) = 1 + \frac{\sin^2\mu + 3\mu\tan\mu}{2}, \tag{29}$$

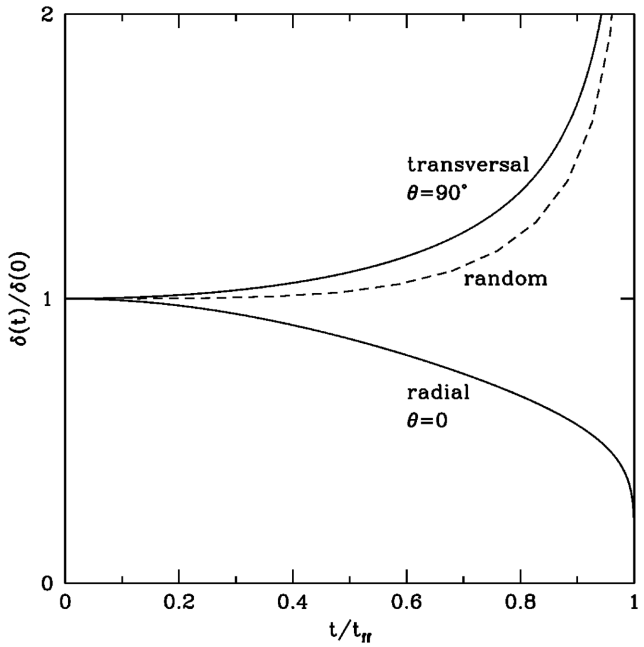

Figure 1. Amplitude of density perturbations during spherical free-fall on a point mass, for perturbations with wavenumber radial ($\theta = 0$) and transversal ($\theta = 90^\circ$). The dashed line shows the evolution of the amplitude for a random distribution of wavenumbers.

where μ is a 'development angle' ranging from 0 to $\pi/2$. The development angle is related to time by

$$t = \frac{2}{\pi}(\mu + \sin\mu\cos\mu)\, t_{\rm ff}, \tag{30}$$

where $t_{\rm ff} = (\pi r_0^3/8GM_\star)^{1/2}$ is the free-fall time of a fluid element initially at a distance r_0 from the star (see Appendix A2 for details). From equation (25), the amplitude of a density perturbation propagating at an angle θ (fixed in the comoving frame) with respect to the radial direction increases as

$$\delta = \delta_0 \left(\frac{\sin^2\theta}{a^2} + \frac{\cos^2\theta}{c^2}\right)^{1/4}, \tag{31}$$

where the scalefactors $a(t)$ and $c(t)$ are given by equation (A10). Fig. 1 shows the evolution of δ for perturbations with wavenumber radial ($\theta = 0$) or transversal ($\theta = 90^\circ$). The dashed line shows the evolution of the amplitude for a random distribution of wavenumbers obtained averaging equation (31) over θ. Since a fluid element contracts in two directions while is stretched in the third, the growth of perturbations is relatively slow: The average amplitude doubles only after 95 per cent of the free-fall collapse of the fluid element has been completed. An even smaller amplification can be expected in the accretion flows on a filament, if the latter is approximated as an infinite cylinder, as contraction in this case only occurs in the direction perpendicular to the filament.

In general, anisotropic collapse and stretching of fluid elements in flows driven by the gravitational field of mass concentrations like stars or filaments dilute and retard the growth of any small-scale density/velocity perturbation initially present in the gas. In the next section we turn to the collapse of a starless, self-gravitating cloud core where the amplification of perturbations is expected to occur at the highest possible rate.

4 APPLICATION TO HOMOLOGOUS COLLAPSE

The dynamics of starless cores appears to be characterized by an overall slow contraction rather than free-fall collapse in their central parts (Keto, Caselli & Rawlings 2015; Campbell et al. 2016). Nevertheless, the simple model of the homologous collapse of a uniform density, pressureless sphere contains the essential characteristics of flows driven by the self-gravity of the gas (Whitworth & Ward-Thompson 2001). In addition, its simplicity allows one to derive analytically the time evolution of the scalefactors needed to apply the formalism of inverse Hubble flows. In this model, the acceleration of the background results from the self-gravity of the core,

$$\nabla' \cdot \boldsymbol{g}_{\rm b} = 4\pi G\rho_{\rm b}, \tag{32}$$

where $\rho_{\rm b} = \rho_0/a^3$, and the scalefactor is

$$a(t) = \cos^2\mu(t), \tag{33}$$

where μ is again given by equation (30) and $t_{\rm ff} = (3\pi/32G\rho_0)^{1/2}$ is the free-fall time (see Appendix A1 for details). In this case equation (17) becomes

$$\frac{{\rm d}^2F}{{\rm d}\mu^2} - 2\tan\mu\frac{{\rm d}F}{{\rm d}\mu} + 6\left(\frac{k'^2}{k_{\rm J,0}^2} - \frac{1}{\cos^2\mu}\right)F = 0. \tag{34}$$

The evolution of density perturbations depends on their initial spatial scale. Consider for example the evolution of small-scale, Jeans-stable perturbations with $k' \gg k_{\rm J,0}$. In a static cloud, such fluctuations oscillate as sound waves with frequency $\omega = c_s k$. If the cloud contracts isotropically with scalefactor a, the size of the perturbation decreases as a (its oscillation frequency increasing accordingly as a^{-1}) but the Jeans length decreases faster, as $c_s/\sqrt{\rho} \sim a^{3/2}$. Thus, any small-scale perturbation that is initially linearly stable and propagates as sound waves becomes gravitationally unstable at some time $t_{\rm gr}(k')$, that approaches $t_{\rm ff}$ as $k' \to \infty$. From equation (34), this time corresponds to $\cos^2\mu_{\rm gr} = k_{\rm J,0}^2/k'^2$. In this limit, the solution of equation (34) is

$$F(\mu) = \frac{1}{\cos\mu}[c_1\sin(p\mu) + c_2\cos(p\mu)], \tag{35}$$

where $p = \sqrt{6}k'/k_{\rm J,0} \gg 1$, representing two oscillating modes (with $F(0) = 0$ and ${\rm d}F/{\rm d}\mu(0) = 0$, respectively). As anticipated by the WKB analysis, the amplitude of the perturbations increase as $1/\cos\mu \propto a^{-1/2}$.

As the contraction of the cloud proceeds, a decreases, and eventually perturbations on scales progressively small become gravitationally unstable. When $k' \ll k_{\rm J,0}$, equation (34) becomes

$$\frac{{\rm d}^2F}{{\rm d}\mu^2} - 2\tan\mu\frac{{\rm d}F}{{\rm d}\mu} - \frac{6}{\cos^2\mu}F = 0. \tag{36}$$

General solution of equation (36) are well known from cosmology (e.g. Narlikar 2002). With the initial conditions appropriate for cloud collapse the solution is (Toalá et al. 2015),

$$F(\mu) = c_1\frac{\tan\mu}{\cos^2\mu} + c_2\frac{2 + \sin^2\mu + 3\mu\tan\mu}{\cos^2\mu}, \tag{37}$$

and represents two growing modes (with $F(0) = 0$ and ${\rm d}F/{\rm d}\mu(0) = 0$, respectively). Asymptotically for $t \to t_{\rm ff}$ both modes grow like $a^{-3/2} \propto (1 - t/t_{\rm ff})^{-1}$ (e.g. Hunter 1962). Perturbations

become gravitationally unstable at a time $t_J(\lambda')$ corresponding to the evolutionary angle

$$\cos\mu_J = \frac{\lambda'}{\lambda_{J,0}}. \quad (38)$$

Thus, in a free-falling background, small-scale and Jeans-stable perturbations are amplified as $a^{-1/2}$ until they become gravitationally unstable and then grow as $a^{-3/2}$, the same rate characterizing the evolution of the parent cloud, which is itself gravitationally unstable ($H \propto (1 - t/t_{ff})^{-1}$).

4.1 Onset of nonlinearity

As the amplitude of the perturbations increases, the linear approximation breaks down at some point. Linear growth terminate when perturbations become Jeans-unstable and collapse or become non-linear at a time t_{nl} and start to dissipate their energy by shocks. After t_{nl} the energy dissipation is extremely rapid, as shocks efficiently convert wave energy into heat.

To evaluate t_{nl}, consider for simplicity a one-dimensional flow. Ignoring pressure and gravity, the momentum equation (7) reduces to

$$\frac{\partial u_1}{\partial t} + \frac{u_1}{a}\frac{\partial u_1}{\partial x'} = -H u_1. \quad (39)$$

With the transformation $v_1 = a u_1$ and $\mathrm{d}\tau = a^{-2}\mathrm{d}t$, equation (39) can be rewritten in the new variables $v_1(x', \tau)$ and τ as the standard (inviscid) Burgers' equation for the static case,

$$\frac{\partial v_1}{\partial \tau} + v_1\frac{\partial v_1}{\partial x'} = 0. \quad (40)$$

The general (implicit) solution of equation (40) is easily obtained with the method of characteristics (see e.g. Jeffrey 2002): a velocity perturbation with initial amplitude $v_1(x', 0) = u_1(x', 0)$ will steepen with time and form a shock at a time $\tau = -\{\min[\mathrm{d}u_1(x', 0)/\mathrm{d}x']\}^{-1} \equiv t_{nl,0}$, where $t_{nl,0}$ is the time for reaching the non-linear stage in the static case. In the presence of contraction, non-linearity therefore occurs at a time t_{nl} such that

$$\int_0^{t_{nl}} \frac{\mathrm{d}\tau}{a^2} = t_{nl,0}. \quad (41)$$

Clearly, in the case of contraction $t_{nl} < t_{nl,0}$, i.e. perturbations enter the non-linear phase earlier than in the static case.

It is straightforward to evaluate t_{nl} in the case of the homologous collapse of a pressureless sphere. A sinusoidal velocity perturbation with wavelength $\lambda' = 2\pi/k'$ and initial amplitude u_0 becomes non-linear and forms a shock at $t = t_{nl}$, corresponding to the evolutionary angle μ_{nl} obtained integrating equation (41),

$$t_{nl,0} = \frac{4t_{ff}}{\pi}\int_0^{\mu_{nl}} \frac{\mathrm{d}\mu}{\cos^2\mu} = \tan\mu_{nl}. \quad (42)$$

For $t_{nl,0} = 1/k'u_0$, this implies

$$\tan\mu_{nl} = \frac{\lambda'}{8t_{ff}u_0}. \quad (43)$$

To compare t_{nl} and t_{gr}, it is convenient to parametrize the amplitude of the perturbations as $u_0 = \mathcal{M}_0 c_s$, where $\mathcal{M}_0$ is the initial value of the rms Mach number, and rewrite equation (43) as

$$\tan\mu_{nl} = \left(\frac{1}{\sqrt{6}\mathcal{M}_0}\right)\frac{\lambda'}{\lambda_{J,0}}. \quad (44)$$

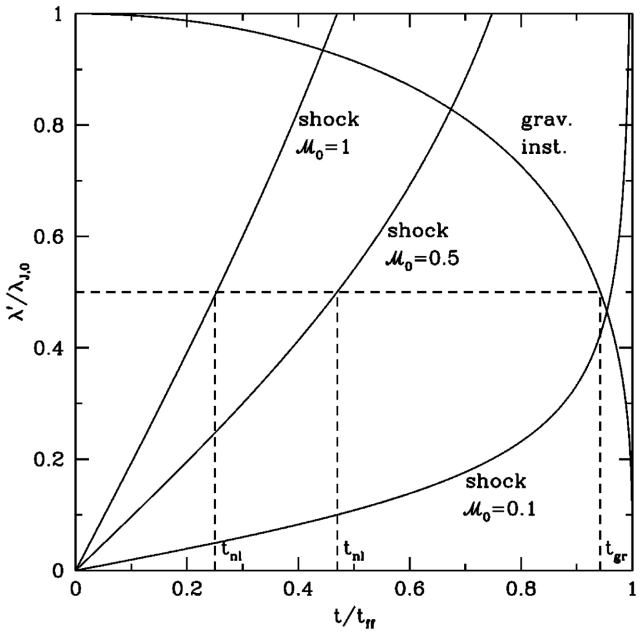

Figure 2. During the collapse of a pressureless cloud, a linear perturbation with comoving wavelength λ' becomes non-linear at a time t_{nl} (*curves labelled 'shock'*) and gravitationally unstable at a time t_G (*curve labelled 'grav. inst.'*). Wavelength is in units of the Jeans wavelength $\lambda_{J,0}$ and time is in units of the cloud's free-fall time t_{ff}. The non-linear time is shown for three values of the initial Mach number of the perturbations, $\mathcal{M}_0 = 1$, $\mathcal{M} = 0.5$ and $\mathcal{M}_0 = 0.1$. The case of $\lambda' = 0.5\,\lambda_{J,0}$ is shown as an example: The non-linear phase is reached before the gravitational instability, unless the perturbations have Mach number below ∼0.1.

Fig. 2 shows the time t_{nl} and t_G at which initially Jeans-stable perturbations become non-linear and gravitationally unstable, respectively, for various values of the rms Mach number representative of the level of non-thermal motions observed in dense cores, where typically $\mathcal{M}_0 \approx 0.1$–1 (Myers 1983, Hacar & Tafalla 2011). Both t_{nl} and t_{gr} are bounded from above by t_{ff}, but depend on the (comoving) scale of the perturbation λ' in opposite ways: t_g increases with decreasing λ', whereas t_{nl} becomes smaller. Thus, perturbations on sufficiently small scales enter the non-linear phase when they are still gravitationally stable. For example, if $\lambda' = 0.5\lambda_{J,0}$, the non-linear stage and the formation of shocks are reached at $t_{nl} = 0.26t_{ff}$ and $t_{nl} = 0.47t_{ff}$ for $\mathcal{M}_0 = 1$ and 0.5, respectively, well before the perturbation becomes gravitationally unstable at $t_G = 0.94\,t_{ff}$.

5 CONTRACTING BOX MODEL

To follow the evolution of small-scale non-self gravitating perturbations up to the non-linear stage in a contracting background we use ECHO, a *shock-capturing* code based on high-order finite-difference methods for the evolution of classic and relativistic magnetized plasmas (Londrillo & Del Zanna 2004; Del Zanna et al. 2007; Landi et al. 2008). The conservative nature of the numerical method employed automatically preserves mass, momentum and total energy density across any fluid discontinuity, so that the appropriate amount of dissipation is introduced at shocks to capture their precise locations and to ensure the correct jump of entropy.

The code works in general coordinate systems, including evolving metrics, so that it can be easily adapted to expanding or contracting numerical boxes, as done recently for a comprehensive study of the non-linear evolution of Alfvén waves in the expanding solar

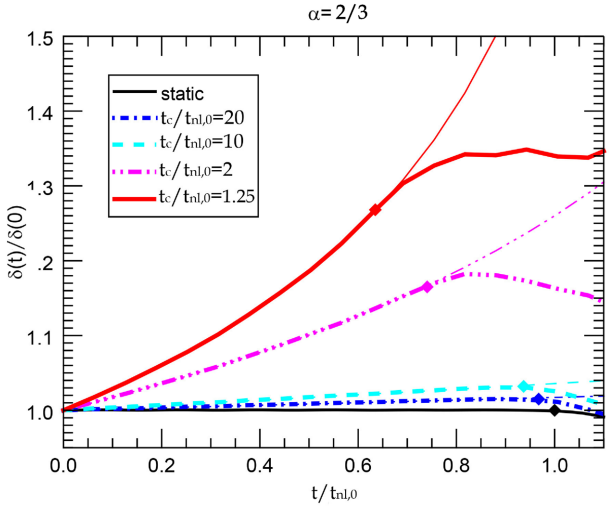

Figure 3. Time evolution of the rms amplitude of density perturbations in a isothermal gas contracting isotropically with the scalefactor of equation (46) with $\alpha = 2/3$ (case of dynamical contraction) for various values of t_c (thick lines). The time is in units of $t_{nl,0}$, the non-linear time for the static model. A diamond marks the position of t_{nl} given by equation (47), and thin lines show the evolution of the amplitude in the WKB approximation. For $t > t_{nl}$ shocks are formed and the waves dissipate.

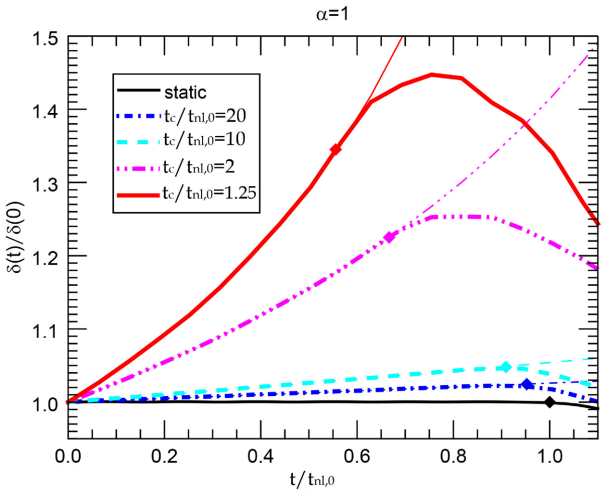

Figure 4. Same as Fig. 3 for $\alpha = 1$.

wind plasma in the case of a uniform background speed (Del Zanna et al. 2015). Here, the method has been extended to any spatial metric of the kind

$$g_{ij} = \mathrm{diag}[a^2(t), b^2(t), c^2(t)], \tag{45}$$

leading to appropriate source terms in the (conservative) hydrodynamics equations containing time derivatives of the above metric functions.

In the simulations, we have assumed an isotropic contraction ($a = b = c$) from $t = 0$ to t_c with scalefactor

$$a(t) = \left(1 - \frac{t}{t_c}\right)^{\alpha}. \tag{46}$$

The range of α of physical interest is $0 < \alpha < 2/3$, which encompasses the case of a static background ($\alpha = 0$), a quasi-static collapse ($0 < \alpha < 2/3$), a dynamical collapse ($\alpha = 2/3$). We also consider the linear case $\alpha = 1$. Figs 3 and 4 show the evolution of the density contrast, normalized to the initial value, for the $\alpha = 2/3$ and $\alpha = 1$, respectively, obtained with a Cartesian box of 512^3 grid points. In the simulations, for a given α we fix the initial amplitude of the perturbations to $\delta_0 = 0.1$ and take as reference time the non-linear time $t_{nl,0}$ for the static case. We then consider various contraction times, $t_c/t_{nl,0} = 20$, 10, 2 and 1.25 and we follow the evolution of perturbations with time. We have run the same simulations with increasing spatial resolutions, observing that for 512^3 grid points convergence was finally achieved. With the scalefactor given by equation (46), the perturbations are expected to become non-linear at a time t_{nl} given by equation (41),

$$\frac{t_{nl}}{t_{nl,0}} = \frac{t_c}{t_{nl,0}} \left\{ 1 - \left[1 - (1 - 2\alpha) \frac{t_{nl,0}}{t_c} \right]^{1/(1-2\alpha)} \right\}. \tag{47}$$

Thus, the decay of perturbations corresponds to the physically correct amount of kinetic energy dissipation compatible with the $\gamma = 1$ adiabatic index adopted in our simulations.

As shown in Fig. 3, the evolution of perturbations depend on the time-scale of the contraction of the box. The growth phase follows strictly the adiabatic approximation $\delta \propto a(t)^{-1/2}$ until non-linear effects result in steepening of the waves and formation of shocks. The analytical expression equation (47) based on the one-dimensional inviscid Burgers' equation predicts the end of the adiabatic phase and the beginning of the dissipative phase, in good agreement with the numerical results. The figure shows that t_{nl} is considerably reduced with respect to the static case if the contraction occurs on a time-scale of the order of a few $t_{nl,0}$. If $t_c \approx t_{nl}$ the amplification due to contraction roughly balances the decay due to dissipation, maintaining an almost constant value of the rms of density (and velocity) perturbations.

6 DISCUSSION AND CONCLUSIONS

We have considered the evolution of small-scale hydrodynamic perturbations in a contracting core, generalizing the analytical approach developed in cosmology for the expanding Universe to the case of arbitrary anisotropic inverse Hubble flows. In general, gravity-driven anisotropic flows, as those characterizing the accretion on to point-like or filament-like mass concentrations are less effective than isotropic flows driven by the self-gravity of a cloud core in the amplification of density and velocity perturbations, due to the diluting effect of the stretching of fluid elements in the direction of the flow.

Even in the isotropic case, however, there are obvious differences with the expanding Universe, where both solenoidal and compressible modes decay because of the expansion of the Universe, leaving only the gravitational instability to promote the formation of sub-structures. In a contracting cloud, solenoidal and compressible perturbations grow with time, the former faster than the latter (as a^{-2} or faster, in the isotropic case), promoting the formation of vortex structures preferentially aligned to the direction of faster contraction. This process may create local enhancements of angular momentum even in the absence of any bulk rotation of the core, and core fragmentation may proceed from the break-up of rotationally supported sub-structures, as found, for example, in the simulations by Goodwin et al. (2004). Conversely, the amplitude of compressible modes in the WKB approximation grows as $a^{-1/2}$ in the isotropic case, conserving the wave action density. These modes couple to the gravitational field, and become gravitationally unstable as the Jeans length progressively shrinks (as long as the collapse is isothermal), leading to fragmentation. However, the

actual fate of compressible perturbations depends, in general, on their wavelength and amplitude, and is controlled by the relative values of several time-scales: the time to reach the non-linear stage $t_{\rm nl}$, the time at which perturbations become gravitationally unstable $t_{\rm gr}$ and the global collapse time-scale of the background. The non-linear time in a collapsing cloud, bounded from above by the free-fall time $t_{\rm ff}$, is shorter than in a static background, and can be estimated analytically on the basis of a one-dimensional Burgers' equation modified by the contraction. For the typical amplitudes of velocity perturbations observed in cloud cores ($\delta u/c_{\rm s} \approx 0.5$–$1$), in general $t_{\rm nl} < t_{\rm gr}$, depending on their wavelength. Only perturbations on scales larger than ∼80–90 per cent of the initial Jeans length (therefore of the order of the size of the core), become Jeans-unstable in the linear phase. The others form shock and start to dissipate their energy, establishing a competition with the 'adiabatic heating' resulting from contraction.

This scenario based on analytical results is supported by fully three-dimensional numerical calculations performed with the hydrodynamical code ECHO. These simulations confirm that initially linear perturbations in a box contracting isotropically increase their amplitude as predicted by the WKB analysis up to the time $t_{\rm nl}$. As shown by the simulations, $t_{\rm nl}$ marks the onset of a phase of decay of the perturbations' amplitude due to strong energy dissipation by shocks. If the rapid amplitude decay following $t_{\rm nl}$ suggested by the numerical calculations is representative of the dissipation in cloud core, it is unlikely that small-scale perturbations can survive to the point of becoming self-gravitating and unstable. Under these circumstances, multiple fragmentation in cores is likely achieved by the growth and subsequent break-up of solenoidal, rather than compressible, small-scale perturbations, either through the fragmentation of disc-like structures (Goodwin et al. 2004), or by the accumulation of mass at the boundary between nearby antiparallel vortices (Clarke et al. 2017). However, it should be kept in mind that vortices are easily disrupted by any large-scale magnetic field due to magnetic stresses associated with current sheets at their edges (Frank et al. 1996; Palotti et al. 2008), an aspect that should be addressed in future works. From the observational side, it would be desirable to exploit the capabilities of submillimetre interferometers like ALMA to constrain the level of fragmentation in starless cores, performing both high-sensitivity dust continuum emission and molecular line observations, to probe the density structure and the vorticity field prior to the formation of a multiple stellar system or a cluster.

ACKNOWLEDGEMENTS

CT acknowledges a CINECA award under the ISCRA initiative (project ISCRA C-TURCOL HP10C3MBH, for the availability of high performance computing resources and support. LDZ and SL acknowledge support from the PRIN-MIUR project prot. 2015L5EE2Y 'Multi-scale simulations of high-energy astrophysical plasmas'. The authors thank Paola Caselli, Roland Grappin, Victor Montagud-Camps, Marco Velli and Malcolm Walmsley for stimulating discussions.

REFERENCES

Bretherton F. P., Garrett C. J. R., 1968, Proc. Roy. Soc., 302, 529
Broderick A., Keto E., 2010, ApJ, 721, 493
Campbell J. L., Friesen R. K., Martin P. G., Caselli P., Kauffmann J., Pineda J. E., 2016, ApJ, 819, 143
Clarke S. D., Whitworth A. P., Duarte-Cabral A., Hubber D. A., 2017, MNRAS, 468, 2489
Davidovits S., Fisch N. J., 2017, ApJ, 838, 118
Del Zanna L., Zanotti O, Bucciantini N., Londrillo P., 2007, A&A, 473, 11
Del Zanna L., Matteini L., Landi S., Verdini A., Velli M., 2015, J. Plasma Phys., 81, 325810102
Dewar R. L., 1970, Phys. Fluids, 13, 2710
Dong Y., Verdini A., Grappin R., 2014, ApJ, 793, 118
Dunham M. M. et al., 2016, ApJ, 823, 160
Falle S. A. E. G., 1972, MNRAS, 156, 265
Fisher R. T., 2004, ApJ, 600, 769
Frank A., Jones T. W., Ryu D., Gaalaas J. B., 1996, ApJ, 460, 777
Goodwin S. P., Whitworth A. P., Ward-Thompson D., 2004, A&A, 414, 633
Goodwin S. P., Kroupa P., Goodman A., Burkert A., 2007, in Reipurth V. B., Jewitt D., Keil K., eds, Protostars & Planets V, Univ Arizona Press, Tucson, AZ, p. 133
Grappin R., Velli M., 1996, J. Geophys. Res., 101, 425
Grappin R., Velli M., Mangeney A., 1993, Phys. Rev. Lett., 70, 2190
Hacar A., Tafalla M., 2011, A&A, 533, A34
Hunter C., 1962, ApJ, 136, 594
Hunter C., 1964, ApJ, 139, 570
Jeffrey A., 2002, Applied Partial Differential Equations: an Introduction, Academic Press, New York
Keto E., Caselli P., 2010, MNRAS, 402, 1625
Keto E., Caselli P., Rawlings J., 2015, MNRAS, 446, 3731
Kirk H. et al., 2017, ApJ, 838, 114
Landi S, Londrillo P., Velli M., Bettarini L., 2008, Phys. Plasmas, 15, 012302
Layzer D., 1963, ApJ, 137, 351
Londrillo P., Del Zanna L., 2004, J. Comp. Phys., 195, 17
Lynden-Bell D., 1973 in Contopoulos G., Henon M., Lynden-Bell D., Geneva Observatory, eds, Dynamical Structure and Evolution of Stellar Systems. p. 92
Mestel L., 1965a, Q. J. R. Astron. Soc., 6, 161
Mestel L., 1965b, Q. J. R. Astron. Soc., 6, 265
Myers P. C., 1983, ApJ, 270, 105
Narlikar J. V., 2002, An Introduction to Cosmology. Cambridge Univ. Press, Cambridge
Olson D. W., Sachs R. K., 1973, ApJ, 185, 91
Palau A. et al., 2017, preprint (arXiv:1706.04623)
Palotti M. L., Heitsch F., Zweibel E. G., Huang Y.-M., 2008, ApJ, 678, 234
Peebles P. J. E., 1980, The Large Scale Structure of the Universe. Princeton Univ. Press. Princeton, NJ
Robertson B., Goldreich P., 2012, ApJ, 750, L31
Rozyczka M., 1983, A&A, 125, 45
Schnee S. et al., 2012, ApJ, 745, 18
Tenerani A., Velli M., 2013, J. Geophys. Res., 118, 7507
Tenerani A., Velli M., 2017, ApJ, 843, 26
Toalá J. A., Vázquez-Semadeni E., Colín P., Gómez G. C., 2015, MNRAS, 446, 3725
Tohline J. E., 1980, ApJ, 239, 417
Verdini A., Grappin R., 2015, ApJ, 808, L34
Whitworth A. P., Ward-Thompson D., 2001, ApJ, 547, 317

APPENDIX A: COLLAPSE AND ACCRETION

A1 Homologous collapse of a pressureless sphere

Consider a cloud of mass M and uniform density ρ_0 collapsing in free-fall. The mass $M(r_0)$ inside a radius r_0 is $M(r_0) = (4\pi/3)\rho_0 r_0^3$, and the free-fall time is $t_{\rm ff} = (3\pi/32G\rho_0)^{1/2}$, independent of the initial radius r_0. The radius of each shell as function of time is given by the parametric solution

$$r = r_0 \cos^2\mu, \qquad t = t_0(\mu + \sin\mu\cos\mu), \tag{A1}$$

where $t_0 = 2t_{\rm ff}/\pi$ and μ is a parameter ('development angle') running from 0 to $\pi/2$. Thus, all shells reach the origin at the same

time, the density increasing uniformly as $\rho = \rho_0/\cos^6\mu$. Thus, in this case,

$$\delta r = \delta r_0 \cos^2\mu, \tag{A2}$$

and the contraction is isotropic with scalefactors

$$a(t) = w(t) = \cos^2\mu(t). \tag{A3}$$

In particular,

$$H(t) = \frac{\dot{a}}{a} = -\frac{\tan\mu}{t_0\cos^2\mu}, \tag{A4}$$

where $t_0 = 2t_{\rm ff}/\pi$.

A2 Free-fall accretion flow

Consider a fluid element free-falling on a star of mass $M_\star$. Let r_0 the position of the fluid element at time $t = 0$ and $u = 0$ its initial velocity. Then its velocity at a radius r is

$$u(r) = -u_{\rm ff}\left(\frac{r_0}{r} - 1\right)^{1/2}, \tag{A5}$$

where $u_{\rm ff} = (2GM_\star/r_0)^{1/2}$. Consider now a shell that at time $t = 0$ ($\mu = 0$) has an outer radius r_0 and an inner radius $r_0 - \delta r_0$, where $\delta r_0 \ll r_0$. If the outer radius of the shell reaches the star in a time $t_{\rm ff} = (\pi^2 r_0^3/8GM_\star)^{1/2}$, the inner radius reaches the star at $t_{\rm ff} - \delta t$, where $\delta t/t_{\rm ff} \approx -3/2(\delta r_0/r_0)$. At any time $t(\mu)$, the parameter of the inner side is $\mu + \delta\mu$, where

$$r_0\,\delta\mu = \frac{3}{2}\left(\frac{\mu + \sin\mu\cos\mu}{1 + \cos 2\mu}\right)\delta r_0. \tag{A6}$$

Thus, while the outer radius of the shell is $r_0\cos^2\mu$, the inner radius is $(r_0 - \delta r_0)\cos^2(\mu + \delta\mu)$ and the thickness of the shell during collapse is

$$\delta r = \left(1 + \frac{\sin^2\mu + 3\mu\tan\mu}{2}\right)\delta r_0. \tag{A7}$$

The radial scalefactor $c(t) = \delta r(t)/\delta r_0$ is then

$$c(t) = 1 + \frac{\sin^2\mu + 3\mu\tan\mu}{2}. \tag{A8}$$

The rate of radial stretching is, after some algebra,

$$\frac{\dot{c}}{c} = \frac{3\mu + (3 + 2\cos^2\mu)\sin\mu\cos\mu}{t_0\cos^3\mu[\cos\mu(4 + \sin^2\mu) + \sin\mu(6\mu + \sin\mu\cos\mu)]}. \tag{A9}$$

On the other hand, the scalefactor in the transversal direction is, as before, $a(t) = b(t) = \cos^2\mu(t)$. Thus, a fluid element in free-fall on a star is stretched in the longitudinal direction and compressed in the transverse direction. When $t \to t_{\rm ff}$, a first-order expansion gives

$$a(t) = b(t) \to \left(1 - \frac{t}{t_{\rm ff}}\right)^{2/3}, \qquad c(t) \to \left(1 - \frac{t}{t_{\rm ff}}\right)^{-1/3}. \tag{A10}$$

and

$$\frac{\dot{a}}{a} \to -\frac{2}{3t_{\rm ff}}\left(1 - \frac{t}{t_{\rm ff}}\right)^{-1}, \qquad \frac{\dot{c}}{c} \to \frac{1}{3t_{\rm ff}}\left(1 - \frac{t}{t_{\rm ff}}\right)^{-1}. \tag{A11}$$

The rate of radial stretching is asymptotically half of the rate of transversal contraction and is asymptotically equal to the radial velocity gradient $\mathrm{d}u/\mathrm{d}r$.

This paper has been typeset from a TEX/LATEX file prepared by the author.